Stability and exchange of subsurface ice on Mars

Norbert Schorghofer and Oded Aharonson
Division of Geological and Planetary Sciences, California Institute of Technology, Pasadena, California, USA

Received 19 August 2004; revised 1 February 2005; accepted 17 March 2005; published 5 May 2005.

[1] We seek a better understanding of the distribution of subsurface ice on Mars, based on the physical processes governing the exchange of vapor between the atmosphere and the subsurface. Ground ice is expected down to $\sim 49^\circ$ latitude and lower latitudes at poleward facing slopes. The diffusivity of the regolith also leads to seasonal accumulation of atmospherically derived frost at latitudes poleward of $\sim 30^\circ$. The burial depths and zonally averaged boundaries of subsurface ice observed from neutron emission are consistent with model predictions for ground ice in equilibrium with the observed abundance of atmospheric water vapor. Longitudinal variations in ice distribution are due mainly to thermal inertia and are more pronounced in the observations than in the model. These relations support the notion that the ground ice has at least partially adjusted to the atmospheric water vapor content or is atmospherically derived. Changes in albedo can rapidly alter the equilibrium depth to the ice, creating sources or sinks of atmospheric H_2O while the ground ice is continuously evolving toward a changing equilibrium. At steady state humidity and temperature oscillations, the net flux of vapor is uninhibited by adsorption. The occurrence of temporary frost is characterized by the isosteric enthalpy of adsorption.

Citation: Schorghofer, N., and O. Aharonson (2005), Stability and exchange of subsurface ice on Mars, *J. Geophys. Res.*, *110*, E05003, doi:10.1029/2004JE002350.

1. Subsurface Ice in Diffusive Contact With Atmospheric Vapor

[2] The Martian atmosphere has low absolute humidity, but due to its low temperature, it is often close to saturation [*Davies*, 1979b]. When water vapor diffuses into the ground, the vapor can freeze out as frost, and ground ice can develop even when in diffusive contact with a "dry" atmosphere. This concept of volatile stability on Mars has been put forward in the seminal work of *Leighton and Murray* [1966]. Later, *Fanale* [1976], *Farmer and Doms* [1979], *Zent et al.* [1986], and *Paige* [1992] provided several conceptional extensions. In a groundbreaking paper, *Mellon and Jakosky* [1993] based the theory of ice stability on diffusion dynamics and produced the first global maps of permanent ground ice stability. Model calculations were subsequently carried out by *Mellon and Jakosky* [1995a, 1995b] and *Mellon et al.* [1997, 2004]. The basic physical processes responsible for ground ice formation are vapor diffusion and deposition. These physical principles alone predict ground ice covered by a dry layer of regolith, as observed by the Gamma Ray Spectrometer (GRS) [*Boynton et al.*, 2002; *Feldman et al.*, 2002; *Mitrofanov et al.*, 2002] on board Mars Odyssey [*Saunders et al.*, 2004]. *Boynton et al.* [2002] and *Mellon et al.* [2004] have argued that vapor exchange between the atmosphere and the subsurface accounts for the geographic distribution of high-latitude ground ice on Mars.

0148-0227/05/2004JE002350$09.00

[3] There are two possible end-member views of subsurface water ice on Mars, which are distinguished by the rate of vapor diffusion between the atmosphere and the subsurface. One is to imagine an atmosphere which has no contact with the subsurface ice buried under an impermeable layer of dry material. Low diffusivities would isolate the subsurface from changes in atmospheric humidity over obliquity variations or other climate changes. The other, contrary view is that the ground ice freely exchanges vapor with the present atmosphere, and is protected by a dry layer of regolith only from large temperature excursions. Ground ice and atmospheric vapor eventually reach an equilibrium. The latter view is supported by (1) theoretical and experimental estimates of effective diffusivities for porous regolith [*Flasar and Goody*, 1976; *Mellon and Jakosky*, 1993; *Hudson et al.*, 2004] and (2) the empirical observation that the geographic boundary of the subsurface ice is correlated with the border line of ice stability for the current climate [*Boynton et al.*, 2002; *Mellon et al.*, 2004]. Here we elaborate on the latter view in which vapor exchanges freely between the atmosphere and the regolith.

[4] For a moment, suppose the ground ice distribution adjusts to orbital variations. If changing the ice depth by 1 meter requires 10^5 years, the average retreat or growth is 10 μm per year. Taking into account the porosity of the subsurface, the average change per Mars year is about the equivalent of the atmospheric water column abundance. If there is substantial redistribution of subsurface ice by diffusion over obliquity cycles, the vapor exchange with the ground ice could have a major impact on the annual atmospheric water budget.

[5] We develop the theory of ice stability, slightly generalizing the approach to permanent stability by *Mellon and Jakosky* [1993], introduce new concepts on temporary frost since the work by *Farmer and Doms* [1979], and deduce concrete consequences for Mars. We present a number of phenomena, some observed and some yet unobserved, which result from the same physical process: water vapor exchange between the atmosphere and the subsurface.

2. Concepts of Stability and Exchange

2.1. Vapor Diffusion and Ice Formation

[6] Frost can form directly from vapor by deposition, without a transient liquid phase. The pertinent pressure is the partial pressure of H_2O which can be lower than the triple point pressure, irrespective of the much heavier atmosphere. On Mars, unlike on Earth, the frost point temperature (typically $\sim$198 K) differs significantly from the melting point ($\sim$273 K).

[7] The frost point temperature is determined solely by the water vapor content, according to the phase diagram of H_2O:

$$p_{sv}(T) = p_t \exp\left(-\frac{H_{\text{subl.}}}{R}\left(\frac{1}{T}-\frac{1}{T_t}\right)\right). \quad (1)$$

Here p_t = 611 Pa and T_t = 273.16 K are the triple point pressure and temperature respectively, H_{subl} = 51,058 J mol^{-1} is the molar heat of sublimation, which only depends weakly on temperature, and R = 8.314 J K^{-1}mol^{-1} is the universal gas constant. The subscript *sv* stands for "solid vapor." The holding capacity of the atmosphere for water vapor, equation (1), strongly dependents on temperature T. Note that salinity does not influence the solid-vapor transition temperature.

[8] Diffusion is due to differences in concentration, temperature, and pressure. The mass flux J in a dilute gas at rest is [*Landau and Lifshitz*, 1987]

$$J = -D\rho_{\text{air}}\left[\frac{\partial}{\partial z}\frac{\rho_v}{\rho_{\text{air}}} + \frac{k_T}{T}\frac{\partial T}{\partial z} + \frac{k_p}{p_{\text{air}}}\frac{\partial p_{\text{air}}}{\partial z}\right], \quad (2)$$

where D is the diffusion coefficient, ρ_{air} is the total density of air, ρ_v is the mass density of water vapor, and z is the vertical coordinate into the ground. The thermodiffusion and barodiffusion ratios k_T and k_p are typically negligible. In a regolith with low permeability, ρ_{air} is constant with depth and the flux is proportional to $\partial\rho_v/\partial z$. In the limit of highly permeable ground, p_{air} is independent of depth and, at low vapor concentrations, the vapor flux is proportional to $\partial p/\partial z$, where p is the partial pressure of H_2O. We assume the vapor flux is described by a gradient in water vapor density ρ_v:

$$J = -D\frac{\partial\rho_v}{\partial z}. \quad (3)$$

[9] Vapor diffuses into regions of low vapor density, irrespective of the relative humidity or saturation of the air. For example, the vapor density of warm, unsaturated air may be higher than that of cold, saturated air. In this case, vapor will flow toward the saturated region and produce frost.

[10] Theoretical estimates for the diffusion coefficient through a porous soil at Martian pressure conditions are typically in the range of 1–20 cm^{2}s^{-1} [*Flasar and Goody*, 1976; *Mellon and Jakosky*, 1993; *Hudson et al.*, 2004].

[11] Mass transfer of H_2O can be caused not only by diffusion, but also by advection. A difference in air pressure causes the gas to move as a whole. Differences in air (CO_2) pressure are caused by thermal expansion and contraction or surface winds. At least on a seasonal basis the contribution of thermal expansion to the vapor transport is small, because the speed of diffusion is high. For a diffusion coefficient of D = 1 cm^{2}s^{-1} and a layer of thickness 100 cm, the vapor percolates at a speed $D/\Delta z$ of 0.01 cm s^{-1} or 36 cm hr^{-1}. This is many orders of magnitude faster than the annual contraction or expansion of air in the ground.

[12] Advection is potentially more important at depths comparable to diurnal skin depths. Very large temperature oscillations in low-thermal inertia material may exceed the validity of the assumed physics of diffusion and, also, air may contribute to heat conduction. Overall, the assumptions appear least certain in regions of very low thermal inertia.

[13] The partial pressure at the planet's surface can be estimated from observations. We assume the partial pressure of H_2O does not change diurnally unless the temperature falls below the frost point, in which case the partial pressure equals the saturation vapor pressure, $p_{\text{surf}} = \min(p_0, p_{sv}(T_{\text{surf}}))$, where p_0 is the partial pressure estimated from afternoon observations. We assume p_0 to be constant throughout the day, as discussed in Appendix C. The same assumption on the behavior of surface humidities is used, for instance, by *Mellon and Jakosky* [1993]. Estimates of p_{surf} require assumptions about the vertical mixing of the atmosphere, from measured column abundances [*Davies*, 1979a; *Jakosky*, 1985; *Clancy et al.*, 1996].

[14] Thermal conduction and vapor diffusion are simulated with a one-dimensional model. As water vapor diffuses through the subsurface, it can undergo phase transitions to free ice or adsorbed H_2O. The thermal model is described in Appendix A, and the diffusion model is described in Appendix B. Similar models have been used by *Flasar and Goody* [1976], *Fanale et al.* [1986], *Mellon and Jakosky* [1993], *Zent et al.* [1993], and *Chamberlain and Boynton* [2004].

[15] Figure 1 shows the accumulation of an ice layer from atmospherically derived water vapor, starting with dry regolith with a thermal inertia $I = \sqrt{k\rho c}$, density ρ, specific heat capacity c, and thermal conductivity k. The temperature varies sinusoidally with an annual period. The partial pressure at the surface never exceeds p_0 and, at times when the atmosphere is saturated, it is lower than p_0. Every year a layer of frost is transported deep into the subsurface where it contributes to a growing ground ice reservoir.

[16] During the long-term evolution, the transition to the ice remains abrupt. The ice content jumps from almost zero (empty) to almost one (full) within one computational grid point. In model simulations initiated with a completely ice filled regolith, a sharp interface retreats to an equilibrium depth. *Mellon and Jakosky* [1993] demonstrated the accumulation of ice from atmospherically derived water vapor beneath a dry layer of regolith. Their transition between the dry and the ice-rich layer spans several numerical layers and

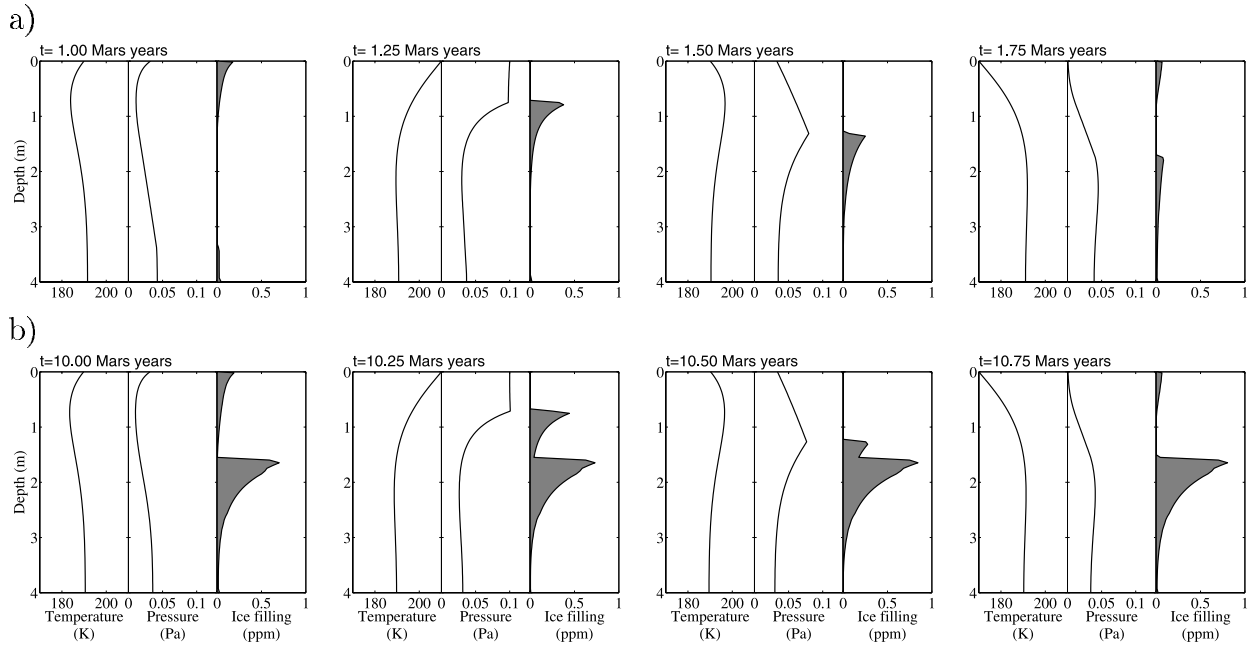

Figure 1. The downward migration of frost over two annual temperature cycles according to a one-dimensional model which simulates the conduction of heat and the diffusion, sublimation, and deposition of water vapor. Each panel shows instantaneous vertical profiles of temperature, partial pressure, and the fraction of pore space filled with ice. (a) The second year and (b) the tenth year after starting with an ice-free regolith. A layer of frost migrates inward during the warming part of the cycle and begins to fill the subsurface with ice. A sinusoidal surface temperature and constant daytime partial pressure are assumed in this model calculation. Model parameters: $p_0 = 0.1$ Pa, $D = 0.1(T/200\ \mathrm{K})^{3/2}\ \mathrm{cm^2 s^{-1}}$, $I = 280\ \mathrm{J\ m^{-2} K^{-1} s^{-1/2}}$, $\rho c = 1.28 \times 10^6\ \mathrm{J\ m^{-3} K^{-1}}$.

is not as abrupt as in our model calculations. This is presumably due to differences in numerical implementation.

[17] Basic physical processes thus lead to a dry layer over an icy layer. The top layer is dry because the large temperature oscillations lead to high vapor densities if any ice is present. The layer "protects" the underlying ice not by reducing vapor transport, but by attenuating temperature oscillations, which would cause a large outward flux of vapor.

2.2. Net Diffusion and Permanent Ice Stability

[18] The mean annual vapor flux is given in terms of the gradient of the mean annual vapor density from averaging equation (3):

$$\langle J \rangle = -\left\langle D \frac{\partial \rho_v}{\partial z} \right\rangle \approx -\langle D \rangle \left\langle \frac{\partial \rho_v}{\partial z} \right\rangle = -\langle D \rangle \frac{\partial \langle \rho_v \rangle}{\partial z}. \qquad (4)$$

Angle brackets $\langle\rangle$ denote time averages. The last equality is valid, because the spatial derivative can be exchanged with the time integral.

[19] The correlation of the diffusion coefficient D with the vapor density gradient $\partial \rho_v / \partial z$ is assumed to be small. In a dilute gas, D is approximately proportional to $T^{3/2}$ for normal diffusion and to $T^{1/2}$ for Knudsen diffusion. Although there is a correlation with temperature, the correlation with temperature gradients or vapor gradients over the period of one year is smaller, because time averaging leads to cancellations of positive and negative contributions.

[20] *Mellon and Jakosky* [1993] have argued that use of the mean vapor density for determining ice stability, rather than a seasonally and diurnally varying vapor density, is justified because diffusion is slow compared to the annual cycle. In steady state, this assumption is unnecessary, because the mean of the gradient is the same as the gradient of the mean in equation (4). The requirement can be dropped and mean values are justified for any diffusion time scale. *Mellon et al.* [1997] discuss an argument along these lines.

[21] In any depth interval without net accumulation of H_2O, the averaged flux $\langle J \rangle$ must be constant with depth, due to mass conservation. The mean flux is constant between the surface and a growing or receding ice reservoir. The mean vapor density $\langle \rho_v \rangle$ must decrease or increase linearly, respectively, with depth. This is true even in the presence of temporary frost or adsorbate, as long as there is no net accumulation of ice or adsorbate at intermediate depths over an annual cycle. The gradient is given by the difference of vapor densities at the boundaries.

[22] Figure 2 shows the amount of subsurface ice as a function of time with and without adsorption. Except for the first few transient annual cycles, when temperature and adsorbate profile are not yet equilibrated, the net accumulation of ice is the same with and without adsorption for an assumed constant porosity. After a long time, adsorption has a negligible impact on the amount of accumulated pore ice. In contrast, the vertical vapor density profile and the amount of periodically exchanged H_2O (breathing) are strongly affected by adsorption [*Jakosky*, 1983, 1985].

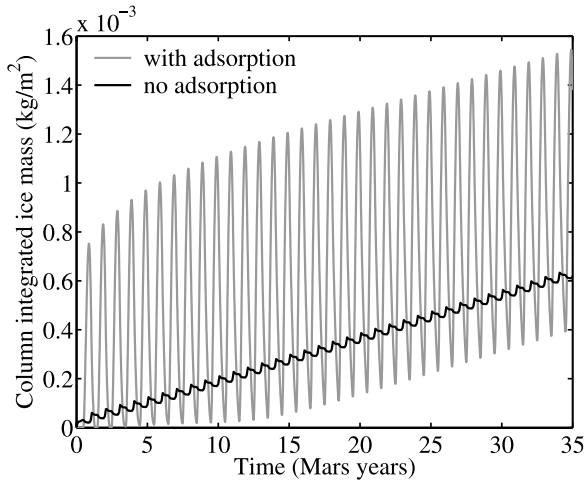

Figure 2. Atmospherically derived ground ice as a function of time with and without adsorption. The regolith is initially ice-free. Although the annual variation in ice content is larger with H_2O adsorption than without, net accumulation is not inhibited by adsorption over long time periods. Model parameters are the same as in Figure 1, and the porosity $\phi = 0.4$. Over short time periods, adsorption can inhibit diffusion between the surface and the ice (not shown in this figure).

[23] The density of adsorbed H_2O is typically large compared to the density of vapor, and adsorption can therefore have a strong influence on the mass balance. It may thus seem surprising that, in a stationary environment, adsorption has no influence on net diffusion. *Zent and Quinn* [1997] and *Tokano* [2003] have suggested that adsorption effectively reduces the diffusion coefficient by many orders of magnitude. The argument is essentially based on the following simplification [e.g., *Jakosky*, 1985; *Zent et al.*, 1993; *Grathwohl*, 2002]. From the mass balance for the vapor and the adsorbed phase:

$$\frac{\partial}{\partial t}(\phi\rho_v + \bar{\rho}_a) = \frac{\partial}{\partial z}\left(\phi D \frac{\partial}{\partial z}\rho_v\right). \tag{5}$$

The density of adsorbed water is denoted by $\bar{\rho}_a$ and ϕ is the porosity of the regolith. If the temperature is independent of time t and depth z, the equation assumes the simpler form

$$\left(1 + \frac{RT}{18\phi}\frac{\partial\bar{\rho}_a}{\partial p}\right)\frac{\partial p}{\partial t} = D\frac{\partial^2 p}{\partial z^2}. \tag{6}$$

The ideal gas law has been used in this derivation. In this simple case, D can be rescaled by the term in parenthesis involving $\partial\bar{\rho}_a/\partial p$. This rescaled diffusion coefficient is relevant for transient diffusion [*Grathwohl*, 2002]. However, for stationary diffusion between two prescribed boundary conditions (the surface and the ground ice) the mean annual flux is given purely by the difference between the mean vapor densities on the surface and the air in immediate contact with any subsurface frost. Neither of these two boundary conditions involves the adsorbate density $\bar{\rho}_a$. As long as the boundary conditions are periodic, adsorption does not inhibit net diffusion. Adsorption changes the instantaneous vertical profile $\rho_v(z)$, but not the mean profile $\langle\rho_v(z)\rangle$.

[24] Since a sharp interface is expected to develop, for receding ground ice as well as for a regolith that accumulates H_2O from an atmosphere with steady humidity, we subsequently employ a two layer model with an ice-free layer on top of an ice-rich layer where pores are completely filled with ice.

[25] Figure 3 shows the result of the diffusion model when the ice table is deeper than the equilibrium depth. In the left-most panel, the breaks in slope in the temperature profiles are caused by the thermal conductivity of ice. The right-most panel shows that the vapor density changes indeed linearly with depth, as required by mass conservation, although temporary frost and a temperature dependent diffusion coefficient are taken into account in these model calculations. The dotted line in Figure 3 shows mean vapor densities deduced from the temperatures on the surface and at the ice table. They are close to the solid line drawn in the same panel, obtained from a detailed simulation of vapor diffusion. Part of the deviation is due to the fact that no computational grid point is placed exactly on the ice table.

[26] The mean flux (4) can be written as

$$\langle J\rangle \approx -\langle D\rangle\frac{\Delta\langle\rho_v\rangle}{\Delta z}, \tag{7}$$

where $\Delta\langle\rho_v\rangle$ is the difference between the mean vapor density at the ice and at the surface, and Δz is the depth of perennial ice below the surface. At the ice, the air is saturated, because it is in contact with the ice. If no frost is present, the vapor pressure can only be lower than p_{sv}.

[27] This line of reasoning leads to a simple and widely valid condition for ground ice stability. The vapor flux

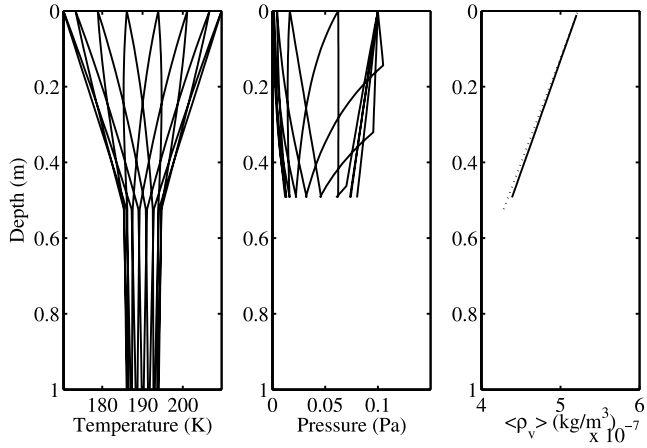

Figure 3. Temperature, partial pressure, and mean vapor density when the ice table is lower (0.5 m) than at equilibrium. A sinusoidal surface temperature with annual period and constant daytime partial pressure are assumed in this model calculation. The vapor density decreases linearly with depth, and the gradient in vapor density drives the ice level to its equilibrium. The dotted lines are estimates of the vapor density using boundary values only. Model parameters: $I = 280$ J m^{-2}K^{-1}s$^{-1/2}$, $\rho c = 1280000$ J m^{-3}K^{-1}, $p_0 = 0.1$ Pa, $D = 1(T/200\text{ K})^{3/2}$ cm^{2}s^{-1}, $\phi = 0.3$.

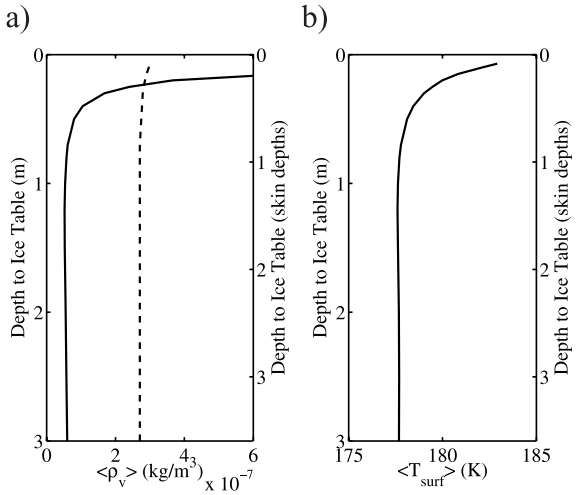

Figure 4. (a) Average vapor density at the ice table (solid line) and on the surface (dashed line) as a function of ice table depth. The equilibrium ice table is located where these two quantities are equal. The burial depth is given in units of meters and in units of seasonal thermal skin depths. (b) Mean annual surface temperature as a function of ice table depth. Surface temperatures increase slightly when the ice enhances the thermal inertia near the surface. Model parameters: latitude, 60°S; $I = 245$ J m^{-2}K^{-1}s$^{-1/2}$; $A_b = 0.2$; $T_{\mathrm{frost}} = 196$ K; $\rho c = 1.28 \times 10^6$ J m^{-3}K^{-1}; $\phi = 0.4$.

between the surface and any point at depth z_0 where frost is present is proportional to the vapor density difference between these two points, $\langle J \rangle \propto \langle p_{\mathrm{surf}}/T_{\mathrm{surf}} \rangle - \langle p_{sv}(z_0)/T(z_0) \rangle$. Ice grows from year to year when

$$\left\langle \frac{p(\mathrm{surface})}{T(\mathrm{surface})} \right\rangle > \left\langle \frac{p_{sv}(\mathrm{at\ depth})}{T(\mathrm{at\ depth})} \right\rangle \tag{8}$$

and is unstable when the inequality is reversed. Equilibrium is reached when the two terms are equal, and the vapor densities balance.

[28] *Fanale* [1976], *Farmer and Doms* [1979], and *Paige* [1992] have determined the depth to the equilibrium ice table by comparing the peak temperature with the frost point on the surface. This may overestimate or underestimate stability. *Leighton and Murray* [1966] and *Mellon and Jakosky* [1993, 1995a] have used a balance of mean partial pressures to determine ice stability. *Mellon et al.* [2004] and this study use mean vapor densities. A balance of mean partial pressures or mean vapor densities can be derived from the physics of diffusion under different assumptions mentioned in section 2.1.

[29] A very cold, fully saturated atmosphere can draw vapor out of the regolith, because the flux is determined by differences in vapor density irrespective of the relative humidity of the air. When the surface is colder than frost in the ground, the absolute atmospheric humidity is lower than the saturated vapor near the ice and vapor will diffuse outward. Since the humidity of a saturated atmosphere cannot increase, the excess water will form surface frost, fogs, or clouds.

[30] The depth to the equilibrium ice table is set by the temperature profile and the annual mean vapor density at the surface. The details of the diffusion and adsorption processes do not influence the long-term H_2O transport and properties of the regolith enter only insofar as they change the thermal profile. For example, the depth to the equilibrium ice table is independent of the diffusion coefficient D, only the rate at which the ice evolves toward this equilibrium depends upon D.

[31] Figure 4 shows annual mean vapor densities as a function of ice table depth (not, as in previous figures, as a function of the z coordinate). Unlike the model calculations above, this simulation includes diurnal temperature variations and uses insolation and bond albedo A_b appropriate for the surface of Mars. Additional details of this model are described in Appendix A. The porosity ϕ determines the volume fraction of ice. The equilibrium ice table is located where the mean vapor density at the ice table and on the surface are equal. The depth to the equilibrium ice table scales with the thermal skin depth.

2.3. Temporary Frost: Isosteric Enthalpy

[32] Permanent stability requires that the escape of vapor on some days be compensated by intake during the remainder of the year. The criterion for permanent stability cannot directly be applied to seasonal stability, using diurnal rather than annual averages, because temperature and pressure conditions do not return to their initial value after one solar day, but a similar argument can be made. If $\Delta\rho_v/\Delta z < 0$, then $\partial\rho_v/\partial z < 0$ at some depth. That is, if the stability condition is satisfied instantaneously, there must be a downward flux of vapor at some depth. For any realistic diffusivity, this will soon lead to the accumulation of frost or adsorbate in the ground.

[33] Figure 5a shows the result of model calculations where ice is seasonally stable but not permanently stable. The solid, black line in Figure 5a indicates the amount of ground frost in the absence of adsorption. Within two solar days after $\min_z \Delta\rho_v < 0$ is first satisfied, ice starts to accumulate and, as expected, continues to exist beyond the duration of inward density differences.

[34] Adsorption typically decreases rapidly with temperature (at constant pressure) and it typically increases with vapor pressure (at constant temperature). The adsorption "isotherm" describes the amount of adsorbed water as a function of pressure, at constant temperature. The "isostere" consists of pressures and temperatures at constant adsorbate mass [*Brunauer*, 1943]. Figure 6 shows examples of adsorption isosteres (dashed lines). The slope of isosteres is described by the isosteric enthalpy $H_{\mathrm{isost.}}$ [*Young and Crowell*, 1962]:

$$\frac{d\ln p}{d(1/T)} = -\frac{H_{\mathrm{isost.}}}{R}. \tag{9}$$

Zent and Quinn [1995] estimate an enthalpy of adsorption of H_2O of 10.4 kJ/mol for their palagonite sample. The enthalpy obtained from equation (B5) [*Jakosky et al.*, 1997] is $H = \epsilon R = 21$ kJ/mol. The enthalpy of sublimation of H_2O is 51 kJ/mol.

[35] Consider a fixed volume of vapor in contact with an adsorbent. If the amount of available water vapor is large compared to the change of adsorbed H_2O mass, then the partial pressure will remain constant with temperature and

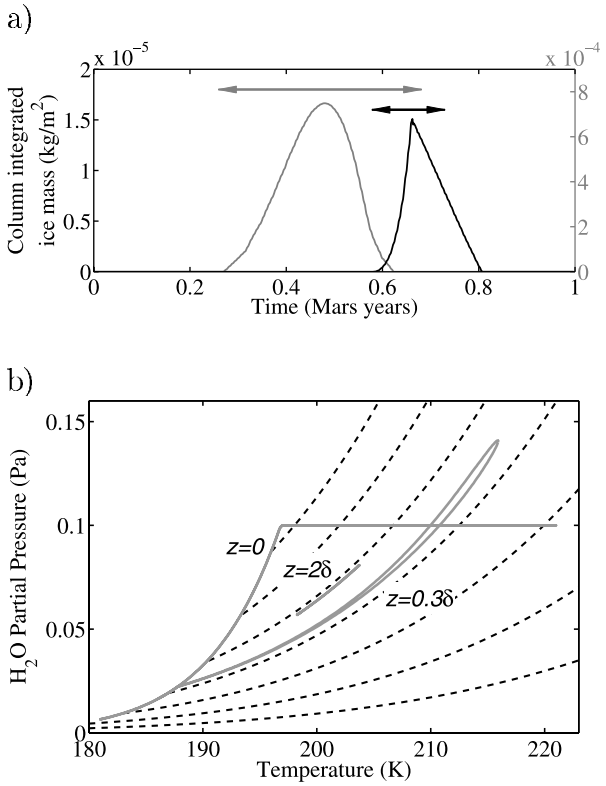

Figure 5. (a) Seasonal subsurface frost in a model calculation over one Martian year. Model parameters are listed in the caption of Figure 1, but the mean temperature is higher. The figure shows the amount of accumulated ice in the absence (black) and presence (gray) of adsorption. Arrows indicate the time period when $\min_z[\rho_{sv}(T(z))] < \rho(\text{surf})$ (black) or when $\min_z[\rho_{sv}(T(z))] < \langle\rho(\text{surf})\rangle$ (gray). (b) Subsurface partial pressures (solid gray lines) in a model calculation with an adsorptive regolith at various depths labeled in units of the thermal skin depth δ. The mean partial pressure is approximately 0.07 Pa. The dashed lines are adsorption isosteres.

adsorption moves along isobars. If, on the other hand, the amount of vapor is small, then little adsorption or desorption can take place and pressures and temperatures follow isosteres. Practically, the behavior will be anywhere between isosteres and isobars, as illustrated in Figure 6. Without additional sources or sinks of H_2O, the pressure cannot change faster with temperature than the slope of the isostere, because this would require simultaneous desorption and decrease in partial pressure. Adsorption is self-limiting because reduction of the partial pressure limits the ability of the soil to adsorb.

[36] If the isosteric enthalpies are significantly smaller than the enthalpy of sublimation, the frost point temperature is reduced little compared to a regolith without adsorption. If the enthalpy of adsorption is higher than for sublimation, free ice can form on warming from water released by desorption.

[37] This principle can be applied to adsorption in the ground, although diffusion contributes to the H_2O balance. Figure 5b shows partial pressures at three different depths in the subsurface from model simulations. Beneath the breathing skin depth, the partial pressure indeed follows isosteres. Hence the partial pressure in the subsurface is known from the isosteres. Frost forms when the isostere intersects the saturation vapor line. For weakly bound water, with a small isosteric enthalpy, temporary frost should be present whenever temperatures in the ground are smaller than the frost point temperature for the mean vapor density, that is, $\rho_{sv}(T(z)) < \langle\rho_v(\text{surf})\rangle$. The mean on the right hand side includes time periods when the atmosphere is saturated and differs in this way from the criterion used by *Farmer and Doms* [1979], who use daytime humidities to estimate seasonal stability. The criterion for frost formation at any depth is $\min_z[\rho_{sv}(T(z))] < \langle\rho_v(\text{surf})\rangle$. Figure 5a shows this criterion roughly captures the time period of seasonal frost, but overestimates the time interval, in part because of the finite enthalpy and in part because the breathing skin depth is not zero. For strongly bound water, frost formation is suppressed due to the slope of the isostere, but we do not estimate this effect here.

[38] Comparing the estimated condition for subsurface frost in the absence of adsorption, $\Delta\rho_v < 0$ somewhere, that is, $\min_z[\rho_{sv}(T(z))] < \rho_v(\text{surf})$, with the estimate when adsorption is large, $\min_z[\rho_{sv}(T(z))] < \langle\rho_v(\text{surf})\rangle$, it is clear that frost is expected under comparable conditions, although timing and vertical distribution of the frost can be substantially different.

3. Consequences of Vapor Diffusion

3.1. Data and Method

[39] Temperatures are obtained with a one-dimensional thermal model of the subsurface, using thermal inertia map [*Putzig et al.*, 2005], albedo map [*Christensen et al.*, 2001], orbital elements [*Allison and McEwen*, 2000], and partial surface pressures obtained from the Thermal Emission Spectrometer (TES) over a Martian year [*Smith*, 2002, 2003]. Since measurements of thermal inertia are based on diurnal temperature variations, they are taken to represent the thermal inertia of the upper, dry layer. The diurnal skin depth is typically on the order of 3 cm. The thermal

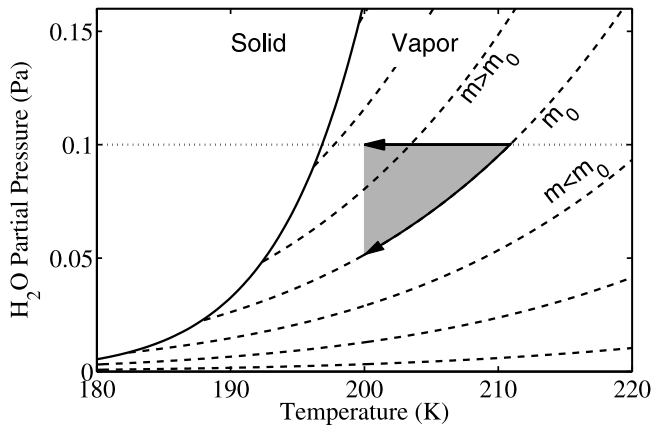

Figure 6. Phase diagram of water (solid line) and adsorption isosteres (dashed lines). Several isosteres corresponding to different adsorbate masses m are shown. The isosteric enthalpy is smaller than the enthalpy of sublimation. In a closed system at equilibrium, partial pressures can be anywhere between isobars and isosteres (shaded area).

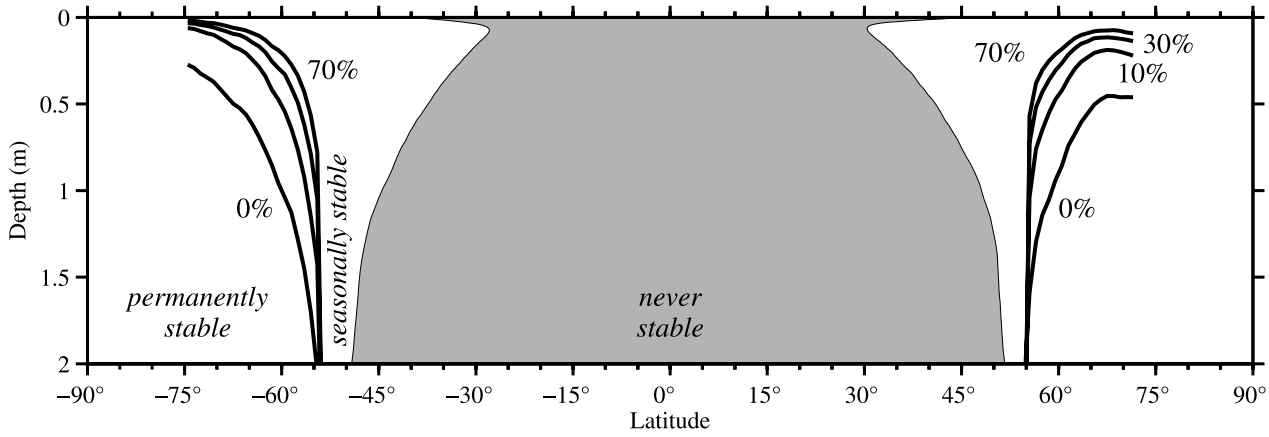

Figure 7. Permanent and seasonal stability for zonally averaged regolith parameters and humidities. The solid lines labeled "0%" indicate depths to permanent stability when no ice is present. When pore spaces are filled with ice at depths where it is stable, the burial depths become shallower than for dry regolith. Burial depths for 0%, 10%, 30%, and 70% volume fraction of ice are shown. No burial depths are plotted at the high latitudes where thermal inertias or humidities from TES are least reliable. In the presence of adsorption, free H_2O frost is not expected within the lightly shaded area at any day of the Mars year.

model includes seasonal CO_2 ice and assumes water vapor or frost beneath the seasonal CO_2 layer.

[40] The surface partial pressure of H_2O is estimated from TES daytime observations [*Smith*, 2002] from March 1999 to March 2001. The conversion of vapor column abundance, usually expressed in precipitable micrometers, to partial pressure of H_2O on the surface depends on the vertical distribution of water vapor. Extraction of surface humidities is described in Appendix C and assumes a well-mixed atmospheric water column up to the H_2O condensation level. According to this approximate analysis the global average surface partial pressure of H_2O is 0.13 Pascal, which corresponds to a frost point of 198 K. This agrees well with previous estimates [*Farmer et al.*, 1977; *Jakosky and Farmer*, 1982]. The average for the northern hemisphere is 0.17 Pascal (200 K) and is 0.09 Pascal (196 K) for the southern hemisphere.

[41] The semi-implicit numerical model simultaneously resolves annual and diurnal temperature cycles. After temperatures have equilibrated, vapor densities are computed from the last Mars year. The equilibrium ice table is determined by first calculating the mean vapor density of saturated air five seasonal skin depths beneath the surface and the mean vapor density at the surface. If ice is stable (that is, the net flux is inward) then a bisection algorithm is employed to search for the equilibrium ice table depth. The calculations include the thermal effect of the ice on the temperature profile, and diurnal as well as seasonal temperature variations are resolved in time and space. Geothermal heating causes a typically negligible increase of mean temperatures with depth, but it may lead to the bisection algorithm failing to identify a stable solution. For this reason, geothermal heating is omitted when ice table depths are computed as a function of latitude or longitude.

3.2. Zonally Averaged Model

[42] Figure 7 shows a stability diagram for zonally averaged thermal inertias, albedos, and humidities. A well-known diagram of this kind has been published by *Farmer and Doms* [1979]. Since depth to permanent ground ice depends on the ice content of the regolith, because the ice changes the thermal properties of the ground, stability boundaries are drawn for several porosities. However, the latitudinal boundary of permanent stability does not depend on ice content.

[43] The ice table retreats rapidly near the latitudinal stability boundary. The reason, as seen in Figure 4, is that at depths large compared to the seasonal skin depth, the vapor density at the ice table is almost independent of depth. Furthermore, the thermal conduction by the ice dampens temperature oscillations in the dry layer and therefore reduces the mean vapor density at the ice table.

[44] The drop in ice table depths at the highest northern latitudes shown in Figure 7 is due to an increase in thermal inertia. Ice is not permanently stable until mean temperatures are at least 6 Kelvin below the mean (daytime) frost point temperature, which demonstrates that such a comparison would overestimate the stability of ground ice.

[45] By recalculating burial depths with hypothetical input parameters, it is possible to separate the effect of thermal inertia, albedo, humidity, and orbital eccentricity on ice stability. If thermal inertia, albedo, and frost point temperature were geographically uniform, the ground ice in the south would extend substantially further equatorward than in the north, because the aphelion passage occurs during southern fall. Mean temperatures at the mid-latitudes would be lower in the south than in the north.

[46] Poleward of 65° latitude, the equilibrium ice table is shallower in the southern hemisphere than in the northern hemisphere, despite low atmospheric humidities in the south. This is primarily due to low thermal inertia at the high southern latitudes.

3.3. Global Distribution of Permanent Ground Ice

[47] Gamma ray and neutron measurements by GRS [*Boynton et al.*, 2004] provide constraints on geographic

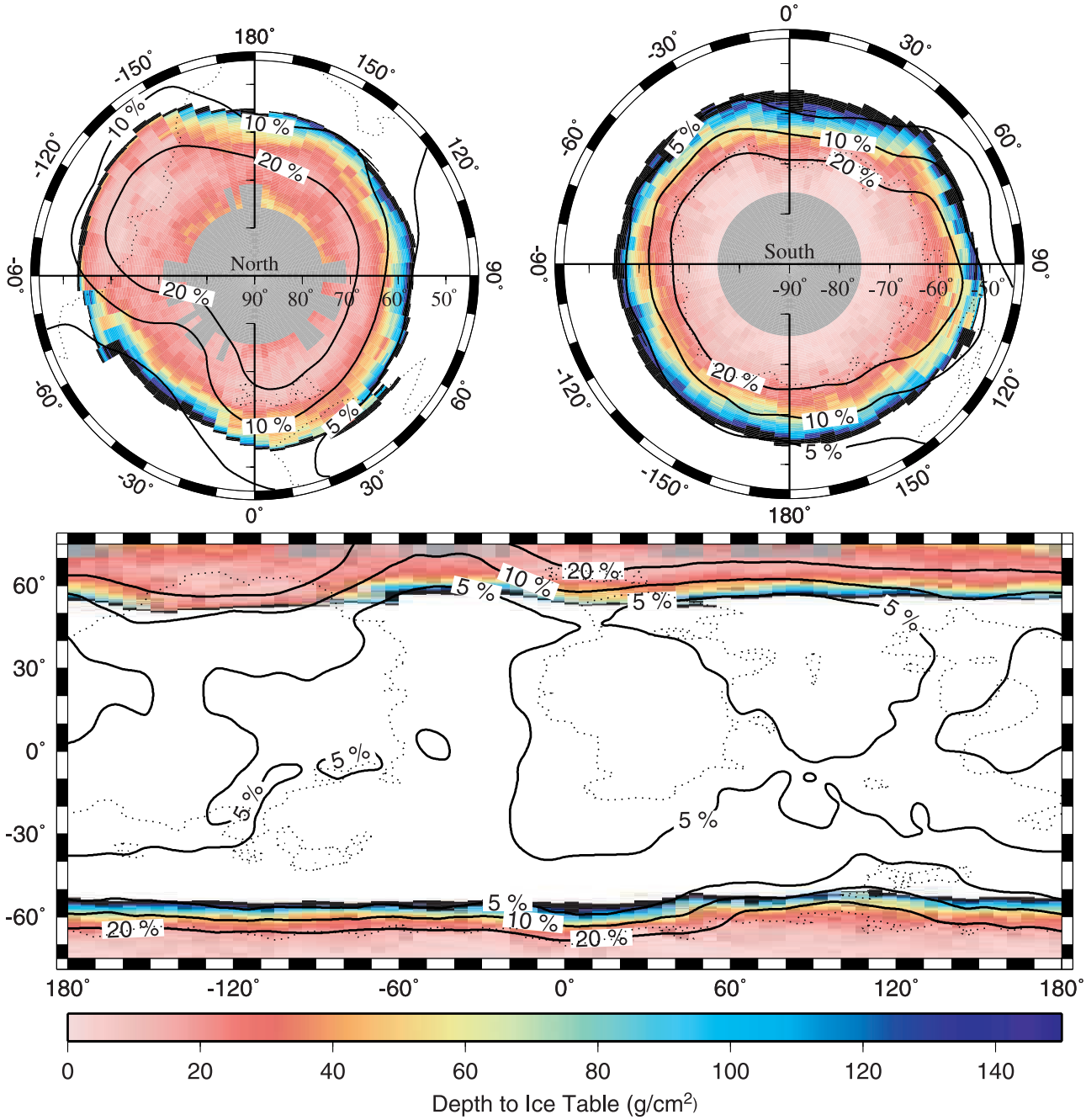

Figure 8. Color indicates depth to the ice table in g cm^{-2} when ice is in equilibrium with the atmospheric water vapor. Ground ice is unstable in the white area. Black segments indicate finite burial depths larger than 150 g cm^{-2}. Missing data points are shown in gray. Assumed volume fraction of ice is 40%, but the geographic boundary between icy and ice-free soil is independent of the ice fraction. Solid contours indicate water-equivalent hydrogen content in percent determined from neutron spectroscopy [*Feldman et al.*, 2004]. The dotted lines are 200 J $m^{-2}K^{-1}s^{-1/2}$ contours of thermal inertia.

distribution and burial depth of ground ice on Mars [*Boynton et al.*, 2002; *Feldman et al.*, 2002, 2004; *Mitrofanov et al.*, 2002; *Tokar et al.*, 2002; *Prettyman et al.*, 2004; *Mellon et al.*, 2004; *Mitrofanov et al.*, 2004] that can be compared with predictions of an equilibrium ice table [*Boynton et al.*, 2002; *Mellon et al.*, 2004]. Data and models are still evolving. For example, neither our subsequent model calculations nor the GRS data extraction takes into account effects related to topographic roughness. Nevertheless, we provide here estimates of the equilibrium ice table and comparisons with observations.

[48] Model predictions are made for ground ice in equilibrium with the water vapor in the present-day atmosphere. The thermal model used by *Mellon et al.* [2004] is potentially more accurate than ours, because the thermal inertia map [*Putzig et al.*, 2005] is derived with the same model

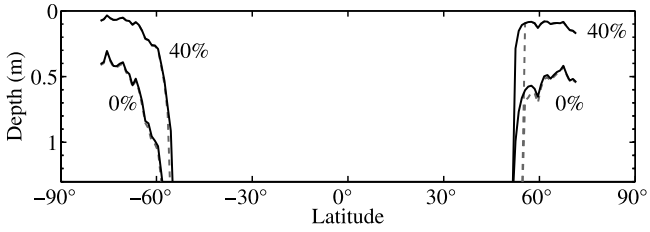

Figure 9. A meridional cross section of the model predictions in Figure 8 (40% ice content) at a longitude of −120°E to −125°E. At this longitude the ground ice disappears rapidly with latitude in the northern hemisphere and burial depths are especially shallow in the southern hemisphere. Equilibrium predictions for 0% ice are also shown. Solid lines are without geothermal heating, and dashed lines are with geothermal heating. The geothermal heating has a negligible effect on the burial depths, but it can cause the bisection algorithm to miss stable solutions.

used to calculate surface temperatures and it includes a more sophisticated atmospheric model. The advantage of our semi-implicit model is that the diurnal cycle is explicitly resolved. We do not create look-up tables and functional fits, but compute stability for each location independently. Humidities are obtained from measurement rather than computed from topography. Annual means of surface vapor densities, which can be much lower than daytime vapor densities due to saturation, are computed by averaging over temperature cycles, rather than using a factor that only depends on latitude. We report depths in terms of mass per area (g cm^{-2}) rather than in terms of distance (cm) to reduce the dependence on assumed regolith densities as described in Appendix A. The neutron and gamma ray flux are also dependent on integrated column mass per area. Figure 8 shows the model predictions (color map) in comparison with water equivalent hydrogen abundance from GRS observations (solid contour lines) [*Feldman et al.*, 2004].

[49] Overall, the predicted burial depths increase equatorward. The lowest latitude at which the model predicts permanent ground ice is ∼49° on both hemispheres and ground ice is expected at all longitudes poleward of ∼57° latitudes. Ice is predicted in 19% of the global area, assuming it continues all the way to the poles. Much of the longitudinal variations of the geographic boundary of ice stability and of the depth to the ice table can be attributed to thermal inertia, as discernible from the dotted contour line in Figure 8, which indicates a thermal inertia of 200 J $m^{-2}K^{-1}s^{-1/2}$. For example, the excursion of ground ice to lower latitudes at −150°E to −90°E occurs in a region where thermal inertia is less than 200 J $m^{-2}K^{-1}s^{-1/2}$. Burial depths at ∼65°S follow a contour of thermal inertia. As discussed in section 3.2, the shallow burial depths at the southern high latitudes are mainly due to low thermal inertia.

[50] The GRS data in Figure 8 show the fraction of water-equivalent hydrogen assuming the elemental composition is uniform with depth (one-layer model) [*Feldman et al.*, 2004]. Dry soil has a hydrogen content of several percent. Other chemical compounds and physically bound water can also contribute to the hydrogen fraction. Burial depths from the model calculations cannot be directly compared with ice content measured from GRS, but the geographic boundary of dry and icy regolith is available from both data sets. The geographic boundary of ground ice in the upper ∼100 g cm^{-2} may be in the range of 5–10% of water-equivalent hydrogen. The footprint of the gamma and epithermal neutron instrument has a diameter of ∼10° (∼600 km), smoothing the spatial distribution.

[51] Immediately after the discovery of ground ice on Mars, it was realized that the southern latitudinal boundary of ice occurrence agrees with predictions of atmosphere-regolith equilibrium [*Boynton et al.*, 2002]. More recently, *Mellon et al.* [2004] have presented a more detailed comparison for the southern hemisphere.

[52] While the zonally averaged southern and northern latitudes of ice stability agree with expectations based on diffusive exchange, and the observed longitudinal variations resemble the model predictions, Figure 8 shows that longitudinal variations in the model are not as pronounced as those measured. This could be due to uncertainties in the input parameters or it may indicate the ice is not fully equilibrated with the atmospheric humidity. Depth dependent thermal inertias, uncertainties in vertical mixing of vapor, contributions from topographic roughness, long term changes in humidity, and the large footprint of the GRS measurements are among sources of errors in the comparison.

[53] In the longitude range from −150°E to −90°E on the northern hemisphere, the predicted ice table disappears abruptly in a region of relatively low thermal inertia. Figure 9 shows burial depths at a longitude in this interval as a function of latitude. The low thermal inertia implies small thermal skin depths, bringing the ice table close to the surface. Furthermore, contributing to the abruptness of the boundary is the strong contrast in thermal conductivity between high inertia ice and the surrounding material. Due to this contrast, the inclusion of even small amounts of ice enhances conduction of heat to depth substantially, attenuating periodic temperature fluctuations and hence lowering the mean vapor density that depends nonlinearly on temperature. This serves as a positive feedback mechanism that sets a sensitive trigger for ice growth in areas of low thermal inertia.

[54] Table 1 (top) lists predicted median burial depths for several latitude bands. Median, rather than mean, values are used, so that formally infinite burial depths for unstable ice can be included. Poleward of 60°S, *Prettyman et al.* [2004] measured 70–85% ice by volume, covered by less than 15 ± 5 g cm^2 of dry material. This agrees well with the corresponding values given in Table 1 (top). The GRS burial depths are obtained from a two-layer model of nuclear scattering and any more detailed vertical distribution of ice is thought to lead to shallower burial depths than 15 ± 5 g cm^{-2}. *Mitrofanov et al.* [2004] determined a column density for the dry soil layer of 16–25 g cm^{-2} in the south from high energy neutrons.

[55] Table 1 (top) shows that in the latitude range of 55°–70° the expected burial depths in the north are comparable to the burial depths in the south in terms of mass per area. Theory argues that burial depths in this latitude range should be at least one diurnal skin depth, even in the north, because ice would retreat extremely rapidly if it was

Table 1. Median Depths of the Equilibrium Ice Table for Current Atmospheric Humidities and Two Different Porosities or Volume Fractions of Ground Ice[a]

	Burial Depth, g cm^{-2}			Burial Depth, g cm^{-2}	
Northern Latitude Range	40% Ice	70% Ice	Southern Latitude Range	40% Ice	70% Ice
55°N–60°N	63	50	55°S–60°S	77	59
60°N–65°N	25	19	60°S–65°S	27	20
65°N–70°N	18	14	65°S–70°S	11	8
	Burial Depth (skin depths)			Burial Depth (skin depths)	
Northern Latitude Range	40% Ice	70% Ice	Southern Latitude Range	40% Ice	70% Ice
55°N–60°N	12	9.1	55°S–60°S	14	10
60°N–65°N	4.8	3.8	60°S–65°S	6.1	4.5
65°N–70°N	3.3	2.4	65°S–70°S	3.3	2.1

[a]The depth to the ice table is set to infinity where ice is unstable. The top part of the table shows depths in terms of mass per area. An ice content of 70% by volume is more realistic than 40%. Equilibrium burial depths are expected to be even shallower poleward of 70°S. The bottom part of the table shows the same data in units of the diurnal skin depth.

shallower. Our minimum equilibrium burial depth for 55°–70°N and 40% ice content is 6 kg m^{-2} or 2.1 diurnal skin depths. For 70% ice content these values change to 4 kg m^{-2} or 1.6 skin depths. We find that ice within a diurnal skin depth experiences high peak temperatures and corresponding vapor densities, which prevent the equilibrium depth from being much closer to the surface than the skin depth of diurnal temperature variations.

[56] Table 1 (bottom) provides predicted burial depths in units of the diurnal thermal skin depth of the dry layer. The seasonal skin depth is ~26 diurnal skin depths. As expected, the depth to the ice table is typically between the diurnal and the seasonal skin depth. Burial depths are sufficiently large that the ice should have only a small influence on thermal inertias determined from diurnal temperature oscillations. The seasonal thermal inertia, on the other hand, should be strongly affected by the presence of the ice and effects the determination of thermal inertias by increasing the mean temperature.

[57] In their pioneering work, *Mellon et al.* [2004] employ a similar thermal model to derive theoretical burial depths. Their minimum burial depths equatorward of 70° are several millimeters. Our burial depths, for 40% ice content, are never less than 1.9 cm, 1.2 times the diurnal skin depth, or 2.0 kg m^{-2} in this latitude range. The assumed thermal inertia of the icy layer is 1318–2013 J m^{-2}K^{-1}s$^{-1/2}$ depending on the thermal inertia of the dry layer, compared to 2290 J m^{-2}K^{-1}s$^{-1/2}$ of *Mellon et al.* [2004]. An ice content of 40% is assumed in both cases. Taking the thermal parameters of *Mellon et al.* [2004] raises the shallowest ice table in our model from a depth of 1.9 cm to 1.3 cm. If, for example, this ice table depth at 37.5°E, 69.5°S is artificially decreased further by a factor of two, to 0.6 cm, the mean vapor density, 1.8×10^{-7} kg m^{-3}, would increase by a factor of 10 at the ice table. The ice would then be unstable at this depth unless the atmospheric humidity was substantially larger such that the frost point was 15 K higher. We conclude that while the discrepancy in minimum burial depths between the models is not large, it cannot simply be attributed to differences in assumed thermal properties.

[58] Figure 10 shows the expected mass fraction of water-equivalent hydrogen in a layer of soil comparable in thickness to the depth to which the GRS measures hydrogen content from epithermal neutrons. This quantity is estimated from calculated burial depths and zonal averages are formed only when values are available for all longitudes. Equilibrium ice table depth and H_2O mass fraction have a hemispheric symmetry up to latitudes of 65° or more. The GRS observes indeed, on a zonal average, a latitudinally symmetric distribution of hydrogen [*Feldman et al.*, 2004]. At individual longitudes, the transition from 5% to 20% water-equivalent hydrogen (in a one-layer model) typically spans 3° in latitude, if the ice is in equilibrium with the atmospheric vapor.

[59] We have recalculated burial depths with a geographically uniform frost point of 198 K, keeping all other parameters the same. The primary effect of geographic variations in surface humidity is to introduce a southward shift of the ground ice distribution by several degrees of latitude in both hemispheres, compared to globally averaged humidity. With a geographically uniform surface humidity, the match between observation and model is not changed significantly.

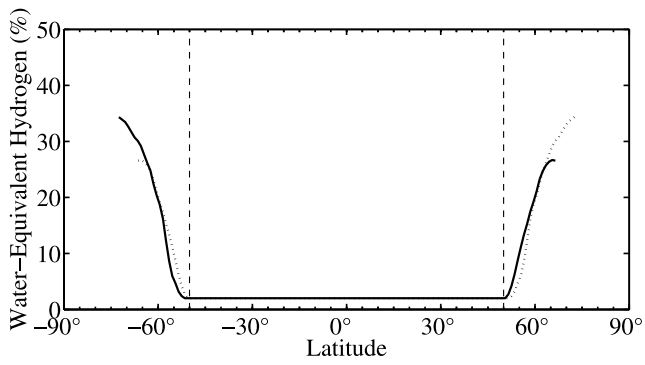

Figure 10. Mass fraction of water-equivalent hydrogen in the upper 100 g cm^{-2} of the subsurface. This quantity can be estimated by GRS using a one-layer model of nuclear scattering. Dry soil is assumed to have 2% water-equivalent hydrogen. The dotted line gives the zonal averages with the sign of latitude reversed, revealing the near-symmetry of the equilibrium ice distribution. The assumed porosity is ϕ = 70% in volume. The H_2O mass is calculated as $h\phi\rho_{ice} + (z_m + h\rho) \times 0.02$, where z_m is the thickness of the dry layer in units of mass per area, ρ_{ice} is the density of bulk ice, ρ is the density of dry regolith, and h is obtained from $h\phi\rho_{ice} + z_m + h\rho$ = 100 g cm^{-2}. Vertical dashed lines are plotted at latitudes of 50°, where a transition in the hydrogen abundance is expected.

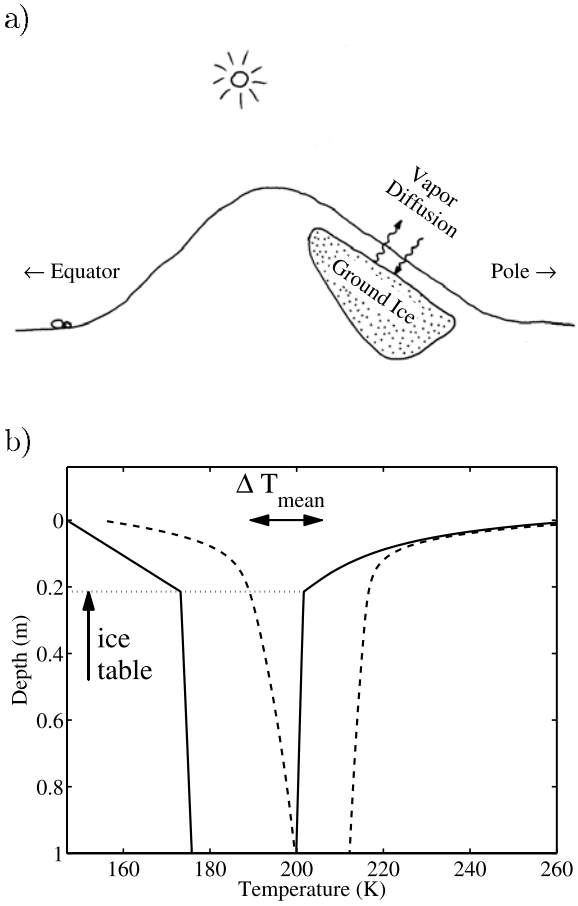

Figure 11. (a) Schematic illustrating ground ice stability beneath a pole-facing slope. (b) Temperature envelopes for a flat surface (dashed lines) and a 30° north-facing slope (solid lines) showing annual maximum and minimum temperatures as a function of depth. Model parameters: $I = 150$ J m^{-2}K^{-1}s$^{-1/2}$, $A_b = 0.3$, $T_{\rm frost} = 198$ K, $\phi = 0.4$.

[60] In summary, model predictions for ice in equilibrium with the atmospheric humidity compare to the observed ground ice distribution as follows. The zonally averaged boundaries of ground ice occurrence are consistent. The longitudinal variations, in both hemispheres, are stronger in the observations than in the model, but bear a clear resemblance. Burial depths of ground ice in the southern hemisphere are consistent with each other.

[61] The correspondence between the observed ground ice distribution and model predictions for ice in equilibrium with the present-day atmospheric humidity provides strong evidence that the ground ice has adjusted to the atmospheric humidity. The ice distribution is coupled to the atmospheric humidity, but it may not be in equilibrium. Current uncertainties, both in model and data, are too large to conclude how close the ice is to its present equilibrium. Ground ice may either have been derived from atmospheric water vapor or the ice has retreated to a depth at which it is stable.

3.4. Modifications of the Ice Distribution

[62] The calculations above assume a flat horizontal surface. Topographic slopes change the amount of insolation substantially. This is accounted for by calculating the incidence angle for arbitrary hour angle, solar declination, and slope azimuth. Furthermore, the horizon for reradiation to space and incoming atmospheric scattering is restricted as described in Appendix A.

[63] Subsurface ice can be permanently stable at lower latitudes due to slope effects, as illustrated schematically in Figure 11a. Figure 11b shows a simulation with model parameters representative of the northernmost Olympus Mons Aureole, where on a 30° pole-facing slope ice is stable. The necessary slopes do not exceed the angle of repose of unconsolidated material and may therefore be common [*Aharonson et al.*, 1998; *Kreslavsky and Head*, 1999]. A global quantitative characterization of the distribution, heterogeneity, and amount of ground ice due to slopes is left for future work.

[64] The environment in which ground ice approaches its equilibrium distribution may be changing gradually. Large changes in albedo have been observed between the Viking missions and Hubble space telescope observations [*Bell et al.*, 1999], and later, Mars Global Surveyor images [*Geissler*, 2005]. In particular, darkening has been observed at high southern latitudes. Figure 12 shows model calculations with a surface albedo that changes from 0.25 to 0.15. In response, the ice table retreats by about 5 cm.

[65] The geographic boundary of the ground ice changes with albedo and the global intake or output of vapor thus ultimately depends on how deep the ice continues below the surface. A well defined estimate of the change in ice volume can be made for latitudes where the equilibrium ice table depth changes only by a finite vertical distance. We compare the ice table depth in the range 60°–65°S using TES albedos to the ice table depth when the albedo is increased by 0.05 everywhere, which may be a realistic albedo change since the Viking period [*Bell et al.*, 1999; *Geissler*, 2005]. The average retreat of the ice due to the darkening is 2.1 cm. The resulting output of water vapor is

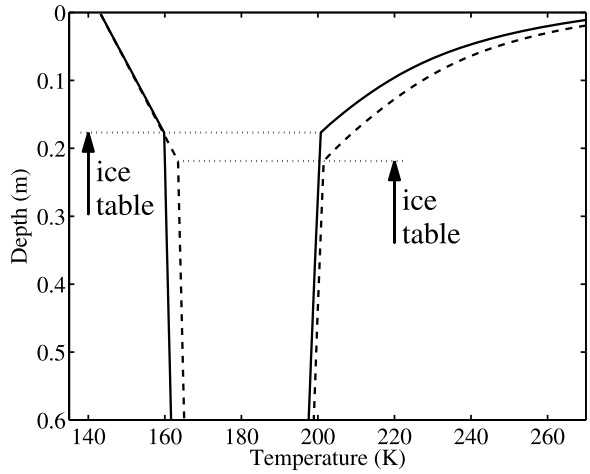

Figure 12. The ice table responds to a change in surface albedo from $A_b = 0.25$ (solid line) to $A_b = 0.15$ (dashed line). Lines show annual maximum and minimum temperatures as a function of depth. The mean temperature increases, and the ice table drops. Model parameters: latitude, 60°S; $I = 245$ J m^{-2}K^{-1}s$^{-1/2}$; $T_{\rm frost} = 200$ K; $\phi = 0.4$.

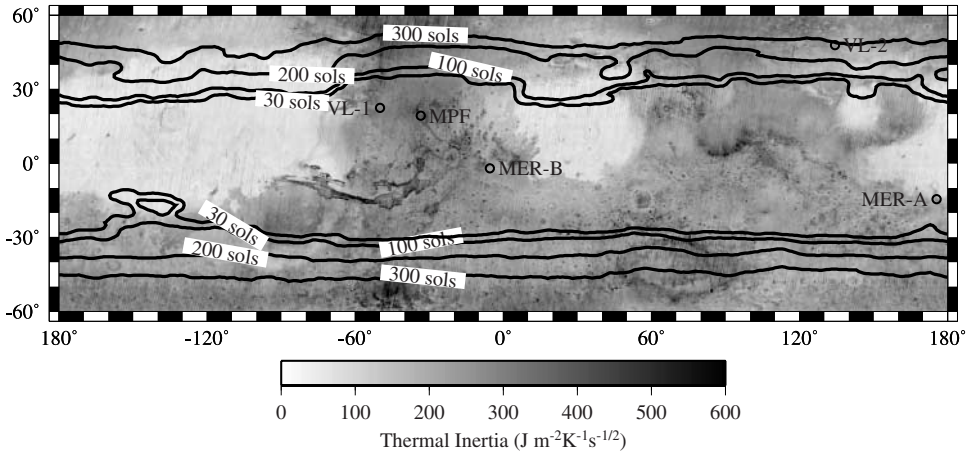

Figure 13. Seasonal subsurface frost for the current climate. The contours indicate the number of solar days per Mars year during which frost is expected in a regolith with weakly adsorbed water. Humidity variations with longitude, latitude, and areocentric longitude [*Smith*, 2002, 2003] are taken into account. Seasonal subsurface frost typically extends to latitudes of about 30°. The grayscale map is thermal inertia [*Putzig et al.*, 2005]. Circles are drawn at past landing sites.

a thousands times larger than the current atmospheric water vapor column abundance. (This assumes an ice content of only 40%.) The time necessary for the ice table to adjust by this amount is far longer than a few decades. We determined the geographically averaged vapor gradient created by the albedo change in this latitude range to be 5×10^{-8} kg m^{-4}, assuming the ice was in equilibrium initially. With $D = 10$ cm^2 s^{-1}, the ice retreat would only be 4 μm yr^{-1}. Hence the ground ice is not expected to reach its equilibrium.

[66] Similarly, not only variations in albedo, but also changes in surface humidity cause intake or release of water vapor and ultimately an adjustment of the ice table. With parameters similar to those used in Figure 12, a doubling of the daytime partial pressure from 0.09 Pa ($T_{\text{frost}} \approx 196$ K) to 0.18 Pa ($T_{\text{frost}} \approx 201$ K) changes the equilibrium ice table depth by ∼5 cm.

[67] Surficial changes of albedo or humidity may occur on relatively short time scales and they can drive changes in the subsurface ice distribution. Hence the ice may be continuously evolving toward a changing equilibrium.

3.5. Global Distribution of Seasonal Subsurface Frost

[68] Due to the exchange of water vapor, seasonally stable regions can accumulate frost. *Farmer and Doms* [1979] found, in a zonal model, that the ground remains below the surface frost point temperature for part of the year at latitudes poleward of 35°S and 46°N. We estimate seasonal stability for an adsorbing regolith with weakly bound water, using the criterion developed in section 2.3. Results for a regolith without adsorption are quantitatively similar.

[69] As was already seen in the zonally averaged model of Figure 7, there are regions where ice is permanently stable, regions where it is seasonally stable, and regions where it is never stable. Permanent stability requires that the escape of vapor on some days be compensated by intake during the remainder of the year. Seasonal frost forms at depth z when the diurnally averaged saturation vapor density falls below the mean annual vapor density on the surface.

[70] A Mars day may be counted as a frost day when the mean annual surface density exceeds the diurnally averaged saturation vapor density at any depth. Figure 13 shows the global distribution of seasonal subsurface frost in the form of a contour map of the number of frost days per Mars year. On this map, the number of frost days is the same as the number of consecutive frost days. Small amounts of frost accumulate during the cold season poleward of ∼30° latitude, in a layer below the penetration depth of diurnal temperature variations and above the penetration depth of seasonal variations.

[71] The amount of seasonal subsurface frost depends upon the diffusivity of the regolith. This seasonal exchange could potentially have global implications for the seasonal water cycle as well as for the mineralogy and hydration state of near surface materials.

3.6. Minimum Diffusivity and Its Consequences

[72] Sublimation, diffusion, and subsurface deposition are ongoing processes on present-day Mars and likely have also governed H_2O distribution during past epochs.

[73] In section 1 it was argued that since the density of ice is far larger than that of water vapor on Mars, even an atmospheric scale-height worth of water vapor corresponds to only tiny changes in the subsurface ice depth. Conversely, when the ground ice is redistributed by sublimation, diffusion, and deposition, it releases and takes up many times an atmosphere's worth of vapor.

[74] Temperatures, and presumably also humidities, vary substantially over obliquity cycles, and enforce a drastically different equilibrium distribution of ice [*Mellon and Jakosky*, 1993]. It is unclear whether the ground ice has adjusted to the present humidity within a single obliquity cycle. The several most recent obliquity cycles had small amplitudes, and even beyond that the obliquity oscillated around a mean value close to the current obliquity of ∼25°. Present-day humidities may happen to coincide

with mean atmospheric conditions of the recent past. However, a significant change in mean obliquities occurred ~4 Myrs in the past [*Touma and Wisdom*, 1993]. Since the distribution of ground ice today appears to have responded to present-day atmospheric humidities, as discussed in section 3.3, there must have been significant ice redistribution within the past 4 Myrs. Assuming an ice table depth change of at least one meter (otherwise we would detect the remnant ice by neutron spectroscopy) within a regolith of 50% porosity, the net diffusive flux over the past 4 Myrs should be at least on the order of $\langle J \rangle \geq O(10^{-4}$ kg m^{-2}yr$^{-1})$.

[75] This flux is an estimated lower limit. If the ice redistributes within a single obliquity cycle, the annual net flux increases to the equivalent of the present atmospheric water vapor column abundance. Also the seasonal exchange, depending on the same diffusion coefficient D, is likely orders of magnitude larger than the net transfer from the permanent ice reservoir. The redistribution of the ground ice alone requires a minimum vapor volume and regolith diffusivity.

[76] Vapor density gradients are limited by the saturation vapor density. If current densities are also representative of the past, $|\Delta\langle\rho_v\rangle\Delta z| = O(10^{-6}$ kg m$^{-4})$, then the diffusion coefficient for the high-latitude regolith needs to be at least $D \geq O(10^{-2}$ cm^{2}s$^{-1})$. Realistic diffusivities easily satisfy this inequality. Diffusivities of $D \geq O(1$ cm^{2}s$^{-1})$ would allow ground ice redistribution within a single obliquity cycle.

[77] Changes in the ground ice distribution require a net transfer of H_2O between the regolith and the atmosphere. The diffusivity required to allow this transfer also implies additional periodic exchange of H_2O. We have not quantitatively estimated the volume of this periodic exchange, but only addressed the net transfer. High diffusivity enhances both types of H_2O transport. Contact with the subsurface ice may also alter the atmospheric deuterium/hydrogen ratio [*Jakosky*, 1991; *Kass and Yung*, 1999].

4. Conclusions

[78] Diffusion and deposition of water vapor produce subsurface frost beneath a dry layer of porous regolith [*Leighton and Murray*, 1966; *Mellon and Jakosky*, 1993]. The soil layer protects underlying ice not primarily by reducing vapor transport, but by attenuating temperature amplitudes. When H_2O transport is predominantly due to gradients in vapor density, it is possible to derive a simple condition for permanent stability of ground ice, shown in equation (8). The equilibrium depth to the ice table is set only by the thermal profile and the mean vapor density on the surface. Permanent ice is typically buried at depths in between the diurnal and seasonal thermal skin depths. Adsorption of H_2O does not affect the net (mean) vapor transfer beyond a transient time period.

[79] The ground ice distribution observed by GRS is compared with model calculations for ice in equilibrium with atmospheric water vapor (Figure 8 and Table 1). The zonally averaged boundaries of ground ice occurrence are consistent. The longitudinal variations in both hemispheres are similar (for the southern hemisphere, see also *Boynton et al.* [2002] and *Mellon et al.* [2004]). Burial depths of ground ice [*Prettyman et al.*, 2004], at least for 60°–70°S, where a comparison can be made, are consistent with each other. Current uncertainties, both in model and data, are too large to conclude precisely how close the ice is to its present equilibrium.

[80] The observed shallow burial depths at high southern latitudes and the lobe of ground ice in the north extending to latitudes of 49°N can both be qualitatively explained by the thermal properties of the low thermal inertia material in these regions. Our model results generally agree with those of *Mellon et al.* [2004], but predict somewhat deeper minimum burial depths.

[81] The relations between present-day humidities and the ground ice distribution indicates that the diffusivity of the regolith is sufficiently large to allow the subsurface ice to respond to the atmospheric humidity. The simplest explanation is that vapor diffusion in the subsurface is very rapid, with a diffusivity on the order of 1 cm^{2}s^{-1} or more, which suggests considerable vapor exchange with the atmosphere today. Alternatively, the present atmospheric conditions represent mean temperature and humidity conditions on Mars for the past several million years. In either case, atmospheric water vapor appears to be the major controlling factor for the observed present-day ground ice distribution.

[82] A number of yet unobserved consequences of vapor exchange are predicted.

[83] Cold (pole-facing) slopes can have permanently stable ground ice where a flat surface at the same latitude is predicted to be free of ice (Figure 11).

[84] If the ground ice is close to equilibrium with the atmospheric vapor, the transition from shallow ice to no ice should span only several degrees of latitude in areas of high thermal inertia, and less in areas of low thermal inertia. Due to the positive thermal feedback, the ice distribution in areas of low thermal inertia is expected to be heterogeneous, adhering strongly to favorable local properties such as surface slope and albedo.

[85] Since the ratio of ice density to vapor density is enormous on Mars, any redistribution of ice requires rapid transfer of water vapor between the atmosphere and the regolith. This exchange could be a sizable contribution to the atmospheric water budget, and is potentially observable today.

[86] The depth to the ice table is sensitive to albedo. Given the ongoing albedo changes on Mars, it is unlikely the ice table has enough time to fully equilibrate.

[87] Seasonal subsurface frost is another consequence of a diffusive regolith. Adsorption isosteres determine the partial pressure in the subsurface. Unless the isosteric enthalpy of adsorption is larger than or comparable to the enthalpy of sublimation, adsorption has little capacity to suppress the formation of free ice. Small amounts of frost accumulate during the cold season down to latitudes of ~30° (Figure 13). Frost is possible on warming for large isosteric enthalpy.

Appendix A: Thermal Model

[88] A one-dimensional diffusion equation for subsurface temperature is solved. The flux boundary condition at the surface includes incoming solar radiation, infrared emission

by the atmosphere, and black body radiation by the surface. Atmospheric emission is approximated by 4% of noontime insolation [*Kieffer et al.*, 1977]. The semi-implicit Crank-Nicholson scheme is unconditionally stable and can therefore simultaneously resolve diurnal and seasonal time scales.

[89] The energy balance for the surface and in the interior requires

$$Q(t) + k(0)\frac{\partial T(z,t)}{\partial z}\bigg|_{z=0} = \left(1 - \frac{\alpha}{\pi}\right)\epsilon\sigma T^4(0,t) + L\frac{\partial m}{\partial t} \quad \text{(A1)}$$

and

$$\rho(z)c(z)\frac{\partial T(z,t)}{\partial t} = \frac{\partial}{\partial z}\left[k(z)\frac{\partial}{\partial z}T(z,t)\right], \quad \text{(A2)}$$

where Q is the incoming solar radiation including the atmospheric contribution, t is time, k is the thermal conductivity, z is the vertical coordinate, α is the slope angle, ϵ is the emissivity, assumed to be 1, σ is the Stefan-Boltzmann constant, L = 590 kJ kg^{-1} is the latent heat of CO_2, and $m(t)$ is the areal mass density of CO_2. The total incoming radiation is

$$Q = \frac{S_0}{R^2}(1 - A_b)\cos i + 0.04\left(1 - \frac{\alpha}{\pi}\right)\sin\beta_{\text{noon}}, \quad \text{(A3)}$$

where i is the incidence angle, S_0 is the solar constant, and R is the distance from the Sun. The factor $(1 - \alpha/\pi)$ takes into account that a tilted surface facing a horizontal horizon sees only a restricted portion of the sky. On a sloped surface the incidence angle i is related to the elevation β of the Sun by

$$\cos i = \cos\alpha\sin\beta - \sin\alpha\cos\beta\cos(\Delta a), \quad \text{(A4)}$$

if cos $i > 0$ and sin $\beta > 0$. Otherwise, cos $i = 0$. The difference in the azimuth of the Sun and the azimuth of the topographic gradient is Δa.

[90] When the surface temperature falls below the sublimation temperature of CO_2 (taken to be 147 K in the low-lying northern hemisphere and 143 K in higher southern hemisphere), then CO_2 forms and the surface temperature remains constant until all the CO_2 has disappeared again. At the bottom boundary we apply a geothermal heat flux of 0.028 W m^{-2}. Latent heat of H_2O sublimation and adsorption is neglected in the model, because the latent heat of ice subliming or deposited over a year is small compared to the total available heat in the same time period.

[91] The presence of ground ice changes the thermal conductivity, heat capacity, and density of the ground. The conductivities of two materials are combined additively, $k = k_{\text{dry}} + \phi k_{\text{ice}}$. The detailed geometry of the ice matrix is not taken into account. Heat conduction by air is neglected. If ρ is the regolith density, c the heat capacity, I the thermal inertia, and ϕ the porosity, then

$$\rho c = \phi\rho_{\text{ice}}c_{\text{ice}} + \rho_{\text{dry}}c_{\text{dry}} \quad \text{(A5)}$$

$$I^2/(\rho c) = \phi k_{\text{ice}} + I_{\text{dry}}^2/\left(\rho_{\text{dry}}c_{\text{dry}}\right). \quad \text{(A6)}$$

Since measurements of thermal inertia are based on diurnal temperature variations, they only represent the thermal inertia of the upper, dry layer. We use c_{dry} = 800 J kg^{-1} K^{-1} and thermal properties of ice near the frost point c_{ice} = 1540 J kg^{-1}K^{-1}, ρ_{ice} = 927 kg m^{-3}, and k_{ice} = 3.2 Wm^{-2}K^{-1} [*Lide*, 2003].

[92] If thermal properties are uniform with depth, the surface temperatures depend only on the thermal inertia and the incoming radiation. Regolith density and heat capacity are required only to determine the skin depth $\delta = I/(\rho c)\sqrt{P/\pi}$, where P is the period of a Mars year. If the depth is expressed in units of mass per area ($\rho\delta$), then ρ cancels. If the conductivity of soil changes with depth, as with ice, a density dependence remains. Following *Mellon and Jakosky* [1993], an empirical relation is used of the form $\rho \approx 150 + 100\sqrt{34.2 + 7.14I}$, where ρ is in units of kg m^{-3} and I is in units of J m^{-2}K^{-1}s$^{-1/2}$.

Appendix B: Diffusion Model With Phase Transitions

[93] As water vapor diffuses through the subsurface, it can undergo phase transitions to free ice or adsorbed H_2O. Conservation of mass requires

$$\frac{\partial}{\partial t}(\bar{\rho}_v + \bar{\rho}_i + \bar{\rho}_a) + \frac{\partial}{\partial z}\bar{J} = 0. \quad \text{(B1)}$$

Subscripts indicate v for vapor, i for free (solid) ice, and a for adsorbed H_2O. The overbar indicates densities and fluxes per total volume, which are related to the actual quantities by factors of regolith porosity ϕ (void space divided by total volume) and the fraction of void space not filled with ice, $1 - \rho_i/\rho_{\text{ice}}$. Here, ρ_i is the ice density in the volume not occupied by regolith and $\rho_{\text{ice}} \approx 926$ kg m^{-3}. Quantities with and without overbar are related by

$$\bar{\rho}_v = (1 - \rho_i/\rho_{\text{ice}})\phi\rho_v \quad \text{(B2)}$$

$$\bar{\rho}_i = \phi\rho_i \quad \text{(B3)}$$

$$\bar{J} = (1 - \rho_i/\rho_{\text{ice}})\phi J, \quad \text{(B4)}$$

where ρ_v is the true vapor density in the void space (not occupied by regolith or ice) and J is the vapor flux through void area. The volume occupied by regolith and ice reduces the diffusion through the factors ϕ and $(1 - \rho_i/\rho_{\text{ice}})$ in equation (B4). Diffusion ceases when the regolith is completely filled with ice. For constant D, the diffusive flux is proportional to the porosity ϕ.

[94] Adsorption in thermodynamic equilibrium is determined by the ambient partial pressure and temperature, that is, the density of adsorbed H_2O can be written as $\bar{\rho}_a = \bar{\rho}_a(p, T)$, where p is the partial pressure of H_2O, after equilibrium is reached. Adsorption is assumed to be rapid compared to temperature variations [*Zent and Quinn*, 1997; *Bish et al.*, 2003].

[95] The model calculations use adsorption isotherms for palagonite powder [*Zent and Quinn*, 1997; *Jakosky et al.*, 1997]:

$$\rho_a = v_m\left(\frac{K_0 p}{e^{-\epsilon/T} + K_0 p}\right)^{0.48}, \quad \text{(B5)}$$

with $K_0 = 1.57 \times 10^{-8}$ Pa^{-1}, $\epsilon = 2573.9$ K, and $v_m = 0.0284\rho$, where ρ is the regolith density. The prefactor v_m depends strongly on the specific surface area of the soil and is considerably smaller for larger grains. For the model calculation in Figure 2, v_m is chosen to be 0.0568 kg/m^3, so that amplitude and mean trend are discernible simultaneously in the figure. For Figure 5, $v_m = 0.568$ kg/m^3, for computational convenience less than a realistic adsorbate density. Since $\bar{\rho}_a$ is still orders of magnitude larger than the vapor density, use of a reduced adsorbate density makes no difference conceptually.

[96] Equations (3), (B1)–(B4), and the ideal gas law lead to

$$\phi \frac{\partial}{\partial t}\left[\frac{p}{T}\left(1-\frac{\rho_i}{\rho_{\text{ice}}}\right)+\frac{R}{18}\rho_i\right]+\frac{R}{18}\left(\frac{\partial \bar{\rho}_a}{\partial p}\frac{\partial p}{\partial t}+\frac{\partial \bar{\rho}_a}{\partial T}\frac{\partial T}{\partial t}\right) = \frac{\partial}{\partial z}\left[\phi D\left(1-\frac{\rho_i}{\rho_{\text{ice}}}\right)\frac{\partial}{\partial z}\frac{p}{T}\right]. \tag{B6}$$

This is an equation for p or ρ_i. If no ice is present, $\rho_i = 0$, and it determines the partial pressure p of H_2O. If ice is present, the partial pressure equals the saturation vapor pressure, $p = p_{sv}(T)$, and the equation determines the change in ice content ρ_i.

[97] The right-hand side of equation (B6) includes the spatial derivatives, which are discretized on the irregularly spaced grid as

$$\partial_z(a\partial_z b)|_j = \frac{a_j b_{j+1}}{h_+(h_- + h_+)} - \frac{a_j b_j}{h_- h_+} + \frac{a_j b_{j-1}}{h_-(h_- + h_+)} + \frac{a_{j-1}(b_{j-1} - b_j)}{h_-(h_- + h_+)} + \frac{a_{j+1}(b_{j+1} - b_j)}{h_+(h_- + h_+)} + O(h_+ - h_-) + O(h_+ + h_-)^2. \tag{B7}$$

The subscript j indicates that the variable is evaluated at depth z_j. Here, $h_+ = z_{j+1} - z_j$ and $h_- = z_j - z_{j-1}$. (A similar discretization is used for the thermal model, but the conductivities are defined in between grid points.)

[98] The time derivative in equation (B6) is discretized as a forward difference. The additional constraint $p \le p_{sv}(T)$ is needed to separate adsorbate-vapor transitions for unsaturated air from ice-vapor transitions in saturated air. The upper boundary condition is given by (1) atmospheric pressure $p(z = 0, t) = p_{\text{atm}}(t)$ and (2) a permeable surface $\rho_{i,0} = 0$. For the lower boundary condition we assume zero vapor flux (impermeable), $J = 0$.

Appendix C: Partial Pressure of H_2O

[99] The conversion of vapor column abundance h, usually expressed in precipitable micrometers, to partial pressure of H_2O at the surface depends on the vertical distribution of water vapor. Mass per area is given by

$$\frac{\text{mass}}{\text{area}} = \int_{\text{surf}}^{\infty} \rho_v(z)dz = h\rho_{\text{liquid}}, \tag{C1}$$

where h is the thickness of the precipitable layer. From the ideal gas law, $p^{H_2O} = \rho_v \frac{R}{18} T$, where $R = 8.314$ J mol^{-1}K^{-1} is the universal gas constant. If the atmosphere is well mixed, then the ratio p^{H_2O}/p^{CO_2}, and therefore ρ_v/ρ^{CO_2}, are independent of height. The vertical density profile of water vapor is proportional to the CO_2 pressure profile. For a hydrostatic atmosphere

$$-\frac{dp^{\text{CO}_2}}{dz} = g\rho^{CO_2}, \tag{C2}$$

where $g = 3.7$ m s^{-2} is surface gravity. Therefore

$$h\rho_{\text{liquid}} = p_{\text{surf}}^{H_2O}\frac{18}{R}\int_0^{H_C}\frac{1}{T(z)}\exp\left(-g\frac{44}{R}\int_0^z\frac{dz'}{T(z')}\right)dz. \tag{C3}$$

H_C is the height of the water vapor condensation level, beyond which the water content is negligible [*Smith*, 2002]. For an isothermal atmosphere $\rho(z) = \rho_{\text{surf}} \exp(-z/H)$, with scale-height $H = RT/(44g)$, and

$$p_{\text{surf}}^{H_2O} = gh\rho_{\text{liquid}}\frac{44}{18}\frac{1}{1-e^{-H_C/H}}. \tag{C4}$$

The estimate only depends on h and H/H_C. For example, $h = 10$ μm and $H_C/H = 2$ correspond to $p_{\text{surf}}^{H_2O} \approx 0.10$ Pa.

[100] The CO_2 pressure is purely determined by the weight of the atmosphere above and barely changes during a diurnal cycle. Due to the assumed mixing of H_2O and CO_2, the partial pressure of H_2O is also constant throughout the day, as long as the atmosphere remains unsaturated. Density variations are caused by thermal contraction and expansion, rather than changes in partial pressure. Hence the isothermal estimate (C4) should be barely affected by temperature changes near the surface. The surface partial pressure $p_{\text{surf}}^{H_2O}$ is at the time of observation. If we think of H_C as the height over which vapor is well-mixed, then H_C/H should not change substantially during a solar day.

[101] We obtain a map of partial pressures at the surface by

$$p_{\text{surf}}^{H_2O}(\lambda, \Phi, L_s) \approx g\rho_{\text{liquid}}\frac{44}{18}\frac{h(\lambda, \Phi, L_s)}{1-e^{-H_C(\lambda, L_s)/H}}, \tag{C5}$$

where λ is latitude and Φ is longitude. We use values of h and H_C from *Smith* [2002] and $H = 11$ km. The mean annual partial pressure at the surface is obtained by

$$\left\langle p_{\text{surf}}^{H_2O}(\lambda, \Phi)\right\rangle = \frac{1}{2\pi}\int_0^{2\pi} p_{\text{surf}}^{H_2O}(\lambda, \Phi, L_s)\frac{dt}{dL_s}dL_s. \tag{C6}$$

The weighting function dt/dL_s takes into account changes in orbital velocity. Missing data in the humidity map are either assumed to be 2 μm during the cold seasons or are filled with averaged neighbor values during the warm seasons.

[102] **Acknowledgments.** It is a pleasure to thank Samar Khatiwala for his work on the thermal model, Bill Feldman and Michael Smith for sharing data in electronic form with us, Mark Simons and Jeroen Tromp for use of their computer clusters, Paul Asimow, David Bish, Troy Hudson, Mike Mellon, and Yuk Yung for insightful discussions, Mimi Gerstell for a careful reading of an earlier version of this manuscript, and Bill Feldman and Bruce Jakosky for helpful reviews. This work was supported, in part, by JPL grant 1250022 and NASA grant NAG5-13326.

References

Aharonson, O., M. Zuber, G. Neumann, and J. Head (1998), Mars: Northern hemisphere slopes and slope distributions, *Geophys. Res. Lett.*, *25*(24), 4413–4416.

Allison, M., and M. McEwen (2000), A post-Pathfinder evaluation of areocentric solar coordinates with improved timing recipes for Mars seasonal/diurnal climate studies, *Planet. Space Sci.*, *48*, 215–235.

Bell, J., M. Wolff, T. Daley, D. Crisp, P. James, S. Lee, J. Trauger, and R. Evans (1999), Near-infrared imaging of Mars from HST: Surface reflectance, photometric properties, and implications for MOLA data, *Icarus*, *138*, 25–35.

Bish, D., J. Carey, D. Vaniman, and S. Chipera (2003), Stability of hydrous minerals on the Martian surface, *Icarus*, *164*, 96–103.

Boynton, W. V., et al. (2002), Distribution of hydrogen in the near-surface of Mars: Evidence for subsurface ice deposits, *Science*, *297*(5578), 81–85.

Boynton, W. V., et al. (2004), The Mars Odyssey Gamma-Ray Spectrometer instrument suite, *Space Sci. Rev.*, *110*, 37–83.

Brunauer, S. (1943), *The Adsorption of Gases and Vapors*, Princeton Univ. Press, Princeton, N. J.

Chamberlain, M., and W. Boynton (2004), Modeling depth to ground ice on Mars, *Lunar Planet. Sci.*, *XXXV*, abstract 1650.

Christensen, P., et al. (2001), Mars Global Surveyor Thermal Emission Spectrometer experiment: Investigation description and surface science results, *J. Geophys. Res.*, *106*, 23,823–23,872.

Clancy, R., A. Grossman, M. Wolff, P. James, D. Rudy, Y. Billawala, B. Sandor, S. Lee, and D. Muhleman (1996), Water vapor saturation at low latitudes around Mars aphelion: A key to Mars climate?, *Icarus*, *122*(1), 36–62.

Davies, D. (1979a), The vertical distribution of Mars water vapor, *J. Geophys. Res.*, *84*(B6), 2875–2879.

Davies, D. (1979b), Relative humidity of Mars' atmosphere, *J. Geophys. Res.*, *84*(B14), 8335–8340.

Fanale, F. (1976), Martian volatiles—Their degassing history and geochemical fate, *Icarus*, *28*(2), 179–202.

Fanale, F., J. Salvail, A. Zent, and S. Postawko (1986), Global distribution and migration of subsurface ice on Mars, *Icarus*, *67*, 1–18.

Farmer, C., and P. Doms (1979), Global seasonal variation of water vapor on Mars and the implications for permafrost, *J. Geophys. Res.*, *84*(B6), 2881–2888.

Farmer, C., D. Davies, A. Holland, D. La Porte, and P. Doms (1977), Mars: Water vapor observations from the Viking orbiters, *J. Geophys. Res.*, *82*, 4225–4248.

Feldman, W. C., et al. (2002), Global distribution of neutrons from Mars: Results from Mars Odyssey, *Science*, *297*(5578), 75–78.

Feldman, W. C., et al. (2004), Global distribution of near-surface hydrogen on Mars, *J. Geophys. Res.*, *109*, E09006, doi:10.1029/2003JE002160.

Flasar, F., and R. Goody (1976), Diurnal behavior of water on Mars, *Planet. Space Sci.*, *24*(2), 161–181.

Geissler, P. E. (2005), Three decades of Martian surface changes, *J. Geophys. Res.*, *110*, E02001, doi:10.1029/2004JE002345.

Grathwohl, P. (2002), *Diffusion in Natural Porous Media*, Springer, New York.

Hudson, T. L., O. Aharonson, N. Schorghofer, M. H. Hecht, N. T. Bridges, and J. R. Green (2004), Water vapor diffusion through porous regolith at Mars environments, *Eos Trans. AGU*, *85*(47), Fall Meet. Suppl., Abstract P41A-0886.

Jakosky, B. M. (1983), The role of seasonal reservoirs in the Mars water cycle. 1. Seasonal exchange of water with the regolith, *Icarus*, *55*(1), 1–18.

Jakosky, B. M. (1985), The seasonal water cycle on Mars, *Space Sci. Rev.*, *41*, 131–200.

Jakosky, B. M. (1991), Mars volatile evolution: Evidence from stable isotopes, *Icarus*, *94*(1), 14–31.

Jakosky, B. M., and C. B. Farmer (1982), The seasonal and global behavior of water vapor in the Mars atmosphere: Complete global results of the Viking atmospheric water detector experiment, *J. Geophys. Res.*, *87*, 2999–3019.

Jakosky, B. M., A. P. Zent, and R. W. Zurek (1997), The Mars water cycle: Determining the role of exchange with the regolith, *Icarus*, *130*, 87–95.

Kass, D., and Y. Yung (1999), Water on Mars: Isotopic constraints on exchange between the atmosphere and surface, *Geophys. Res. Lett.*, *26*(24), 3653–3656.

Kieffer, H., T. Martin, A. Peterfreund, B. Jakosky, E. Miner, and F. Palluconi (1977), Thermal and albedo mapping of Mars during the Viking primary mission, *J. Geophys. Res.*, *82*, 4249–4291.

Kreslavsky, M., and J. Head (1999), Kilometer-scale slopes on Mars and their correlation with geologic units: Initial results from Mars Orbiter Laser Altimeter (MOLA) data, *J. Geophys. Res.*, *104*(E9), 21,911–21,924.

Landau, L. D., and E. M. Lifshitz (1987), *Fluid Mechanics*, Elsevier, New York.

Leighton, R., and B. Murray (1966), Behavior of carbon dioxide and other volatiles on Mars, *Science*, *153*, 136–144.

Lide, D. (Ed.) (2003), *CRC Handbook of Chemistry and Physics*, 84th ed., CRC Press, Boca Raton, Fla.

Mellon, M. T., and B. M. Jakosky (1993), Geographic variations in the thermal and diffusive stability of ground ice on Mars, *J. Geophys. Res.*, *98*(E2), 3345–3364.

Mellon, M. T., and B. M. Jakosky (1995a), The distribution and behavior of Martian ground ice during past and present epochs, *J. Geophys. Res.*, *100*(E6), 11,781–11,799.

Mellon, M. T., and B. M. Jakosky (1995b), Correction to the distribution and behavior of Martian ground ice during past and present epochs, *J. Geophys. Res.*, *100*(E11), 23,367–23,370.

Mellon, M. T., B. M. Jakosky, and S. E. Postawko (1997), The persistence of equatorial ground ice on Mars, *J. Geophys. Res.*, *102*(E8), 19,357–19,369.

Mellon, M. T., W. C. Feldman, and T. H. Prettyman (2004), The presence and stability of ground ice in the southern hemisphere of Mars, *Icarus*, *169*, 324–340, doi:10.1016/j.icarus.2003.10.022.

Mitrofanov, I. G., et al. (2002), Maps of subsurface hydrogen from the high-energy neutron detector, Mars Odyssey, *Science*, *297*(5578), 78–81.

Mitrofanov, I. G., et al. (2004), Soil water content on Mars as estimated from neutron measurements by the HEND instrument onboard the 2001 Mars Odyssey Spacecraft, *Sol. Syst. Res.*, *38*(4), 253–265.

Paige, D. A. (1992), The thermal stability of near-surface ground ice on Mars, *Nature*, *356*(6364), 43–45.

Prettyman, T. H., et al. (2004), Composition and structure of the Martian surface at high southern latitudes from neutron spectroscopy, *J. Geophys. Res.*, *109*, E05001, doi:10.1029/2003JE002139.

Putzig, N. E., M. T. Mellon, K. A. Kretke, and R. E. Arvidson (2005), Global thermal inertia and surface properties of Mars from the MGS mapping mission, *Icarus*, *173*, 325–341.

Saunders, R., et al. (2004), 2001 Mars Odyssey mission summary, *Space Sci. Rev.*, *110*, 1–36.

Smith, M. D. (2002), The annual cycle of water vapor on Mars as observed by the Thermal Emission Spectrometer, *J. Geophys. Res.*, *107*(E11), 5115, doi:10.1029/2001JE001522.

Smith, M. D. (2003), Interannual variability in TES atmospheric observations of Mars during 1999–2003, *Icarus*, *167*, 148–165.

Tokano, T. (2003), Spatial inhomogeneity of the Martian subsurface water distribution: Implication from a global water cycle model, *Icarus*, *164*, 50–78.

Tokar, R. L., W. C. Feldman, T. H. Prettyman, K. R. Moore, D. J. Lawrence, R. C. Elphic, M. A. Kreslavsky, J. W. Head III, J. F. Mustard, and W. V. Boynton (2002), Ice concentration and distribution near the south pole of Mars: Synthesis of Odyssey and Global Surveyor analyses, *Geophys. Res. Lett.*, *29*(19), 1904, doi:10.1029/2002GL015691.

Touma, J., and J. Wisdom (1993), The chaotic obliquity of Mars, *Science*, *259*, 1294–1297.

Young, D., and A. Crowell (1962), *Physical Adsorption of Gases*, Butterworths, London.

Zent, A., F. Fanale, J. Salvail, and S. Postawko (1986), Distribution and state of H_2O in the high-latitude shallow subsurface of Mars, *Icarus*, *67*, 19–36.

Zent, A. P., and R. C. Quinn (1995), Simultaneous adsorption of CO_2 and H_2O under Mars-like conditions and application to the evolution of the Martian climate, *J. Geophys. Res.*, *100*(E3), 5341–5349.

Zent, A. P., and R. C. Quinn (1997), Measurement of H_2O adsorption under Mars-like conditions: Effects of adsorbent heterogeneity, *J. Geophys. Res.*, *102*(E4), 9085–9095.

Zent, A. P., R. M. Haberle, H. C. Houben, and B. M. Jakosky (1993), A coupled subsurface-boundary layer model of water on Mars, *J. Geophys. Res.*, *98*(E2), 3319–3337.

O. Aharonson and N. Schorghofer, Division of Geological and Planetary Sciences, California Institute of Technology, MC 150-21, Pasadena, CA 91125, USA. (norbert@gps.caltech.edu)